# Tunable Magnonic Thermal Hall Effect in Skyrmion Crystal Phases of Ferrimagnets

Se Kwon Kim, Kouki Nakata, Daniel Loss, and Yaroslav Tserkovnyak

Phys. Rev. Lett. **122**, 057204 — Published 6 February 2019

DOI: 10.1103/PhysRevLett.122.057204

# Tunable Magnonic Thermal Hall Effect in Skyrmion Crystal Phases of Ferrimagnets

Se Kwon Kim,[1,2] Kouki Nakata,[3] Daniel Loss,[4,5] and Yaroslav Tserkovnyak[1]

[1] *Department of Physics and Astronomy, University of California, Los Angeles, California 90095, USA*
[2] *Department of Physics and Astronomy, University of Missouri, Columbia, Missouri 65211, USA*
[3] *Advanced Science Research Center, Japan Atomic Energy Agency, Tokai, Ibaraki 319-1195, Japan*
[4] *Department of Physics, University of Basel, Klingelbergstrasse 82, CH-4056 Basel, Switzerland*
[5] *RIKEN Center for Emergent Matter Science (CEMS), Wako, Saitama 351-0198, Japan*

(Dated: January 16, 2019)

We theoretically study the thermal Hall effect by magnons in skyrmion crystal phases of ferrimagnets in the vicinity of the angular momentum compensation point (CP). To this end, we start by deriving the equation of motion for magnons in the background of an arbitrary equilibrium spin texture, which gives rise to the fictitious electromagnetic field for magnons. As the net spin density varies, the resultant equation of motion interpolates between the relativistic Klein-Gordon equation at CP and the nonrelativistic Schrödinger-like equation away from it. In skyrmion crystal phases, the right- and the left-circularly polarized magnons with respect to the order parameter are shown to form the Landau levels separately within the uniform skyrmion-density approximation. For an experimental proposal, we predict that the magnonic thermal Hall conductivity changes its sign when the ferrimagnet is tuned across CP, providing a way to control heat flux in spin-caloritronic devices on the one hand and a feasible way to detect CP of ferrimagnets on the other hand.

*Introduction.*—Magnetic skyrmions are swirling spin textures, which are characterized by the topological skyrmion number defined in terms of the real-space spin configuration [1]. Their topological characteristic influences not only the dynamics of themselves, e.g., by engendering the Magnus force, but also the dynamics of electrons moving through them [2]. For example, when ferromagnetic skyrmions form a crystal lattice, electrons whose spin follows the local spin texture adiabatically experience the Lorentz force due to the fictitious magnetic field proportional to the skyrmion density and thereby exhibit the so-called topological Hall effect [3]. Recently, there has been a growing interest in skyrmions in antiferromagnets [4] and ferrimagnets [5–7] because of their faster dynamics and smaller sizes compared to ferromagnetic counterparts, which can enable high-speed and high-density spintronic devices [8, 9]. Electronic transport properties of an antferromagnetic skyrmion crystal have been investigated as well theoretically [10–14], showing fundamental differences from those of ferromagnets such as the absence of the topological Hall effect.

Magnons, which are quanta of spin waves [15], can transport information and exhibit topological phenomena similarly to electrons. Their potential ability to realize devices based on insulating magnets, which are free from drawbacks of conventional electronics such as significant energy loss due to Ohmic heating, has led to the emergence of magnon-based spintronics [16]. In skyrmion crystal phases of ferromagnets, magnons have been shown to experience the fictitious magnetic field by keeping their spin antiparallel to the local spin texture [17]. As a result, magnons form the approximate Landau levels with the finite Berry curvature [18], causing the thermal Hall effect [19–21]. However, the magnon bands and their transport properties in antiferromagnetic skyrmion crystals have not been studied.

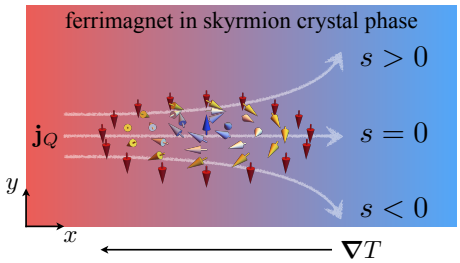


FIG. 1. Schematic illustration of the magnonic heat flux $\mathbf{j}_Q$ through a ferrimagnet in its skyrmion crystal phase subjected to a temperature gradient $\nabla T$. The colored small arrows depict a single skyrmion texture of the order parameter $\mathbf{n}$. Magnons can exhibit the thermal Hall effect since the skyrmion crystal gives rise to the fictitious magnetic field, which magnons of left and right circular polarization (with respect to the order parameter) experience as if they carry the positive and the negative charge, respectively. The induced transverse heat flux changes its direction as the net spin density $s$ along $\mathbf{n}$ varies across 0.

In this Letter, we fill this gap by investigating a theoretically more general problem: The dynamics of magnons in the presence of skyrmion crystals in ferrimagnets exhibiting the angular momentum compensation point (CP) [22], at which the net spin density vanishes, but the magnetization can be finite. One class of such ferrimagnets is rare-earth transition-metal alloys such as GdFeCo or CoGd whose net spin density can be tuned by varying either temperature [23] or chemical composition [24]. To this end, we start by deriving the equation of motion for magnons in the presence of an arbitrary spin texture, which includes the fictitious electromagnetic field. The obtained equation of motion is reduced to the nonrelativistic Schrödinger-like equation for ferro-

magnetic magnons away from CP and to the relativistic Klein-Gordon equation for antiferromagnetic magnons at CP, interpolating between the dynamics of ferromagnets and that of antiferromagnets as previously shown for the dynamics of domain walls and skyrmions [25, 26]. In the presence of a skyrmion crystal, two species of magnons with right and left circular polarization (with respect to the order parameter) will be shown to experience the fictitious magnetic fields of opposite directions and form the Landau levels separately, realizing two-dimensional magnonic topological insulators [27]. As an experimental proposal, we will show that the thermal Hall conductivity changes its sign as the ferrimagnet is tuned across CP. See Fig. 1 for a schematic illustration. One promising platform is offered by GdFeCo films, where isolated skyrmions have been observed [5] and the antiferromagnetic domain-wall dynamics has been demonstrated at CP [25]. The proposal provides not only a feasible way to control the direction of the thermal flux, which can be useful in spin caloritronics [28], but also a thermal transport measurement for determining CP, which can complement the other methods based on magnetic resonances [23, 29] or domain-wall speed measurements [25].

*General formalism.*—Our model system is a collinear ferrimagnet with potential energy density given by [26]

$$\mathcal{U}[\mathbf{n}] = A(\boldsymbol{\nabla}\mathbf{n})^2/2 + D\mathbf{n}\cdot(\boldsymbol{\nabla}\times\mathbf{n}) - \mathbf{h}\cdot\mathbf{n}\,, \qquad (1)$$

where $\mathbf{n}(\mathbf{r},t)$ is the three-dimensional unit vector representing the direction of the magnetic order. Here, the first term is the exchange energy; the second term is the Dzyaloshinskii-Moriya interaction (DMI), which exists when the inversion symmetry is broken [30]; the last term represents the Zeeman coupling between the external field $\mathbf{h}$ and the magnetization along the direction of the order parameter. Here, we are neglecting the other terms such as the dipolar interaction by following the previous literature on chiral magnets [31]. With a suitable choice of the coefficient values, the ground state is a skyrmion crystal [31]. The equilibrium order-parameter configuration will be denoted by $\mathbf{n}_0$.

The dynamics of the order parameter $\mathbf{n}$ of the ferrimagnet can be described by the following Landau-Lifshitz-like equation [25, 26, 32]:

$$s\dot{\mathbf{n}} + \rho\mathbf{n}\times\ddot{\mathbf{n}} = \mathbf{n}\times\left(A\nabla^2\mathbf{n} - 2D\boldsymbol{\nabla}\times\mathbf{n} + \mathbf{h}\right)\,, \qquad (2)$$

where $s$ is the equilibrium spin density and $\rho$ parametrizes the inertia associated with the dynamics of the order parameter [33]. The left-hand side is the time derivative of the net spin density, $\mathbf{s} = s\mathbf{n} + \rho\mathbf{n}\times\dot{\mathbf{n}}$, the former and the latter of which are the longitudinal and the transverse component of the spin density with respect to the order parameter, respectively [34]. Conventional ferromagnets and antiferromagnets have only the first and the second term, respectively, on the left-hand side.

To obtain the equation of motion for a magnon, which is a quantum of small-amplitude fluctuations from the equilibrium state, we use the local coordinate system $\mathbf{n}'$, where the equilibrium state is in the positive $z$ direction, $\mathbf{n}'_0 \equiv \hat{\mathbf{z}}$ [19, 35]. The transformation can be implemented by a three dimensional rotation matrix $\mathcal{R}$ satisfying $\mathbf{n}_0 = \mathcal{R}\mathbf{n}'_0$. We will use one explicit realization of it in this work: $\mathcal{R} = \exp(\phi_0\mathcal{L}_z)\exp(\theta_0\mathcal{L}_y)$ for $\mathbf{n}_0 = (\sin\theta_0\cos\phi_0, \sin\theta_0\sin\phi_0, \cos\theta_0)$ where $\mathcal{L}_y$ and $\mathcal{L}_z$ are the generators of the rotations about the $y$ and the $z$ axis, respectively [36].

The equation of motion for magnons can be obtained from Eq. (2) to linear order in the fluctuation $\delta\mathbf{n}' \equiv \mathbf{n}' - \hat{\mathbf{z}} = n'_x\hat{\mathbf{x}} + n'_y\hat{\mathbf{y}}$. Since the equation is second order in time derivative, there are two types of solutions. It is convenient to represent the two monochromatic solutions with the complex fields: $\psi_+ = n'_x - in'_y \propto \exp(-i\epsilon t/\hbar)$ for right-circularly polarized magnons and $\psi_- = n'_x + in'_y \propto \exp(-i\epsilon t/\hbar)$ for left-circularly polarized magnons where $\epsilon$ is the magnon energy. We will refer the former and the latter to the positive-chirality ($q = 1$) and the negative-chirality ($q = -1$) solutions, respectively. The equation of motion for a magnon of chirality $q$ is given by

$$-qs\left(i\partial_t - \frac{q\phi}{\hbar}\right)\psi_q + \rho\left(i\partial_t - \frac{q\phi}{\hbar}\right)^2\psi_q = A\left(\frac{\boldsymbol{\nabla}}{i} - \frac{q\mathbf{a}}{\hbar}\right)^2\psi_q\,, \qquad (3)$$

which is our first main result. See Supplemental Material for its derivation [37]. Here, $\phi$ is the texture-induced scalar potential given by $\phi = \hbar(\mathcal{R}^{-1}\partial_t\mathcal{R})_{12} = -\hbar\cos\theta_0\partial_t\phi_0$, where the subscript 12 denotes a corresponding matrix element of $\mathcal{R}^{-1}\partial_t\mathcal{R}$. The vector potential consists of two contributions [19]: $\mathbf{a} = \mathbf{a}^t + \mathbf{a}^d$, where the first term is from the exchange energy, $a^t_i = -\hbar(\mathcal{R}^{-1}\partial_i\mathcal{R})_{12} = \hbar\cos\theta_0\partial_i\phi_0$, and the second term is from the DMI, $\mathbf{a}^d = -(\hbar D/A)\mathbf{n}_0$. The texture-induced fictitious electric and magnetic fields are given by

$$e^t_i = -\partial_i\phi - \partial_t a^t_i = \hbar\mathbf{n}_0\cdot(\partial_t\mathbf{n}_0\times\partial_i\mathbf{n}_0)\,, \qquad (4)$$

$$b^t_i = \epsilon_{ijk}\partial_j a^t_k = (\hbar/2)\epsilon_{ijk}\mathbf{n}_0\cdot(\partial_k\mathbf{n}_0\times\partial_j\mathbf{n}_0)\,, \qquad (5)$$

in the Einstein summation convention. The obtained fields are identical to those for electrons [2, 38] and magnons [19, 35] in ferromagnets. The DMI-induced vector potential $\mathbf{a}^d$ gives rise to another contribution to the fictitious fields, $\mathbf{e}^d = -\partial_t\mathbf{a}^d = (\hbar D/A)\partial_t\mathbf{n}_0$ and $\mathbf{b}^d = -(\hbar D/A)\boldsymbol{\nabla}\times\mathbf{n}_0$ [19]. Note that the chirality $q = \pm 1$ of a magnon serves as its charge with respect to the electromagnetic fields, which can be understood as follows. Since the positive- and negative-chirality magnons carry spin whose directions are locked parallel and antiparallel with respect to the background spin texture $\mathbf{n}_0$ [39], they pick up the Berry phase with the opposite signs and experience the opposite fictitious electromagnetic fields [40]. During the derivation, we neglected the second and higher order terms in $\phi$ and $\mathbf{a}$ and the term proportional to the external field, by focusing on high-energy magnons whose wavelength is much smaller

than the spatial extension of the texture and whose kinetic energy dominates the Zeeman energy, which we will refer to as the exchange approximation [41].

At CP, the equilibrium spin density vanishes, $s = 0$, and the nature of the dynamics becomes antiferromagnetic. The equation of motion is then reduced to the following Klein-Gordon equation [42] which describes the dynamics of a relativistic particle with charge $q$ in the presence of an electromagnetic field:

$$(i\hbar\partial_t - q\phi)^2 \psi_q = c^2 \left(\frac{\hbar}{i}\boldsymbol{\nabla} - q\mathbf{a}\right)^2 \psi_q \,, \tag{6}$$

where $c \equiv \sqrt{A/\rho}$ is the characteristic speed that is the magnon speed in the absence of electromagnetic fields. This equation describing the dynamics of magnons in antiferromagnets moving through a general spin texture has not been derived before except for a special case of a one-dimensional domain wall [39, 42].

When sufficiently distant from CP, a ferrimagnet has enough spin density $s$ to neglect the inertial term $\propto \rho$ in Eq. (2) for the low-energy dynamics. The equation of motion (3) for ferrimagnetic magnons is then reduced to that for ferromagnetic magnons [19, 35]:

$$-\operatorname{sgn}(qs) i\hbar\partial_t \psi_q = \left[\frac{1}{2m}\left(\frac{\hbar}{i}\boldsymbol{\nabla} - q\mathbf{a}\right)^2 - \operatorname{sgn}(s)\phi\right]\psi_q \,, \tag{7}$$

with the effective mass $m = \hbar|s|/2A$, which resembles the Schrödinger equation for a nonrelativistic charged particle subjected to an electromagnetic field.

It is instructive to discuss the solutions to Eq. (3) in the absence of the scalar and the vector potentials $\phi = 0$ and $\mathbf{a} = \mathbf{0}$, which are given by the plane-wave solutions, $\psi_q \propto \exp(i\mathbf{k}\cdot\mathbf{r} - i\epsilon t/\hbar)$ [43]. The energy-momentum relation is given by

$$\epsilon_q(\mathbf{k}) = \sqrt{(mc^2)^2 + \hbar^2 c^2 \mathbf{k}^2} + \operatorname{sgn}(qs) mc^2 \,. \tag{8}$$

The solution to Eq. (6) for an antiferromagnetic magnon is given by the high-kinetic energy limit, i.e., $\hbar|\mathbf{k}| \gg mc$: $\epsilon_\pm \approx \hbar c|\mathbf{k}|$. The two solutions are degenerate at the level of approximation taken in Eq. (6) where the time reversal symmetry is respected by having vanishing spin density $s = 0$. The lower-energy solution to Eq. (7) for a ferromagnetic magnon is given by the low-kinetic energy limit, i.e., $\hbar|\mathbf{k}| \ll mc$: $\epsilon_q \approx \hbar^2\mathbf{k}^2/2m$ with the chirality $q = -\operatorname{sgn}(s)$. Note that spin of the low-energy magnons is locked antiparallel to the direction of the background spin density $s\mathbf{n}_0$. Here, the momentum scale governing the separation between a nonrelativistic and a relativistic regime is given by $mc = \hbar|s|/2\sqrt{A\rho}$.

*Magnon in a skyrmion crystal.*—Now, let us apply the above formalism to one specific example: Magnons in a skyrmion crystal of a quasi-two-dimensional ferrimagnet. We will assume that the skyrmion crystal is static, for

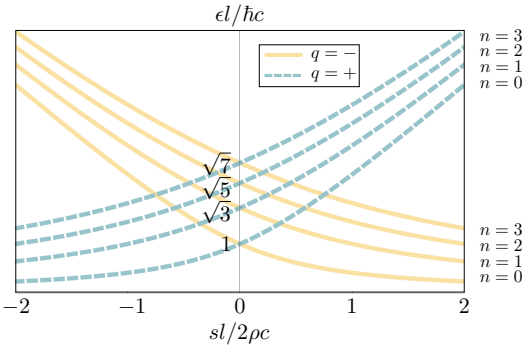


FIG. 2. The plot of the Landau levels [Eq. (11)] of magnon bands in ferrimagnetic skyrmion crystals in terms of the rescaled energy $\epsilon l/\hbar c$ and the rescaled spin density $sl/2\rho c$. The solid gold and the dashed blue lines represent the right-circularly polarized ($q = +$) and the left-circularly polarized ($q = -$) magnon bands, respectively.

which the fictitious electric field vanishes. A skyrmion is characterized by its integer skyrmion number [44]:

$$Q = \frac{1}{4\pi}\int dxdy\, \mathbf{n}_0 \cdot (\partial_x \mathbf{n}_0 \times \partial_y \mathbf{n}_0) \equiv \int dxdy\, \rho_{sky} \,, \tag{9}$$

counting how many times the order parameter $\mathbf{n}_0$ wraps the unit sphere. Under suitable conditions, skyrmions can crystalize in a triangular lattice as observed in several materials [2], giving rise to the finite skyrmion number density per unit area, which we denote by $\rho_{sky}$. The associated fictitious magnetic field [Eq. (5)] is given by

$$\mathbf{b}^t = -4\pi\hbar\rho_{sky}\hat{\mathbf{z}} \,. \tag{10}$$

The spatial profile of the magnetic field depends on the detailed values of material parameters, making it cumbersome to take into account analytically. Therefore, below, we will account for its effects by spatially averaging it: $\mathbf{b} = -4\pi\hbar\langle\rho_{sky}\rangle\hat{\mathbf{z}}$ [37]. The corresponding magnetic length is given by $l = \sqrt{\hbar/|b_z|} = 1/\sqrt{4\pi|\langle\rho_{sky}\rangle|}$, which is proportional to the distance between neighboring skyrmions. The DMI-induced contribution $\mathbf{b}^d$ vanishes after spatial averaging. In addition, we will assume the negative skyrmion density $\rho_{sky} < 0$ and thus $b_z > 0$ without loss of generality for subsequent discussions.

To solve Eq. (3), we adopt the known results for the Landau levels of a nonrelativistic charged particle subjected to a uniform magnetic field [36, 45]. Plugging the monochromatic function, $\psi_q(\mathbf{r}, t) = \exp(-i\epsilon t/\hbar)\psi_{nn'}(\mathbf{r})$ into Eq. (3), where $\psi_{nn'}(\mathbf{r})$ is the known eigenfunction of the right-hand side of Eq. (3) for the $n$th Landau level ($n'$ is the index for states within each Landau level), yields the following solutions:

$$\epsilon_n^q = \sqrt{(mc^2)^2 + \hbar c^2 b_z(2n+1)} + \operatorname{sgn}(qs) mc^2 \,. \tag{11}$$

These magnon bands in a ferrimagnetic skyrmion crystal within the approximation of the uniform skyrmion density is our second main result. The number of states

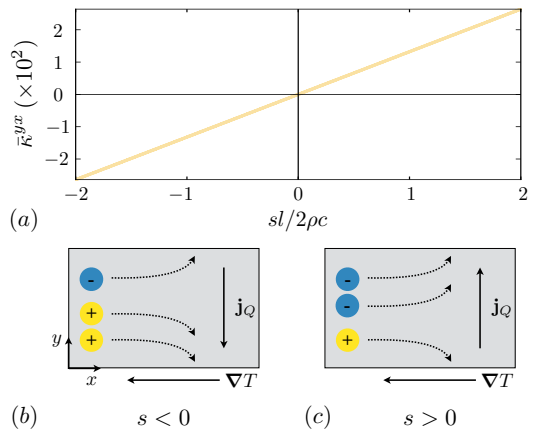


FIG. 3. (a) The plot of the rescaled thermal Hall conductivity $\bar{\kappa}^{yx} \equiv (2\pi\hbar t/k_B^2 T)\kappa^{yx}$, which parametrizies the ratio of the induced transverse heat flux $j_Q^y$ to the applied longitudinal temperature gradient $\partial_x T$ for the ferrimagnet film of thickness $t$. (b) and (c) the schematic illustrations of the positive-chirality (+) and the negative-chirality (−) magnon motions subjected to a temperature gradient $\boldsymbol{\nabla} T = (\partial_x T)\hat{\mathbf{x}}$ and the resultant transverse energy flux $\mathbf{j}_Q = j_Q^y \hat{\mathbf{y}}$.

in one Landau level is given by the total number of the fictitious magnetic flux quanta through the plane, which is twice the total number of skyrmions in the system. The massless relativistic limit is given by $\epsilon_n^{\pm} \approx c\sqrt{\hbar b_z(2n+1)}$, which agrees with the known result for the Klein-Gordon equation [46]. The lower band in the massive limit, $mc^2 \gg c\sqrt{\hbar b_z(2n+1)}$, is reduced to the solution for nonrelativistic particles: $\epsilon_n \approx (\hbar b_z/2m)(2n+1)$. The solution can be cast into the dimensionless form in terms of the rescaled energy $\xi \equiv \epsilon l/\hbar c$ and the rescaled spin density $\zeta \equiv sl/2\rho c$: $\xi_n^{\pm} = \sqrt{\zeta^2 + 2n + 1} \pm \zeta$. See Fig. 2 for the plot. The solid gold and the dashed blue line represent the right-circularly polarized ($q = +$) and the left-circularly polarized ($q = -$) magnon bands, respectively.

*Tunable thermal Hall effect.*—Each flat Landau level of magnons [19, 20] has the Chern number $\nu_0 = -q$, which is the integral of the uniform Berry curvature defined in terms of the magnonic wavefunction over the Brillouin zone [36]. Such magnons can give rise to the thermal Hall effect [47, 48], a phenomenon of generation of a transverse energy flux $j_Q^y$ upon the application of a longitudinal temperature gradient $\partial_x T$: $j_Q^y = -\kappa^{yx}\partial_x T$, which is quantified by the thermal Hall conductivity $\kappa^{yx}$ [49]. Within the linear response theory, the thermal Hall conductivity for our case is given by $\kappa^{yx} = (k_B^2 T/2\pi\hbar t)\sum_n [c_2(\rho^B(\epsilon_n^-)) - c_2(\rho^B(\epsilon_n^+))]$, where $t$ is the thickness of the ferrimagnet, $c_2(x) = (1+x)(\log(1+x^{-1}))^2 - (\log x)^2 - 2\mathrm{Li}_2(-x)$, $\mathrm{Li}_2(z)$ is the polylogarithm function, and $\rho^B(\epsilon) = [\exp(\epsilon/k_B T) - 1]^{-1}$ is the Bose-Einstein distribution [47]. Figure 3(a) shows the plot of the rescaled thermal Hall conductivity $\bar{\kappa}^{yx} \equiv (2\pi\hbar t/k_B^2 T)\kappa^{yx}$ as a function of the rescaled spin density $\zeta = sl/2\rho c$. The plot is drawn with the following value for the ratio of the characteristic relativistic energy scale to the temperature: $\hbar c l^{-1}/k_B T \sim 0.11$, which is obtained from the magnon speed $c \sim 10^4$ m/s calculated for GdFeCo [26], the magnetic length $l = 1/\sqrt{4\pi|\langle\rho_{sky}\rangle|} \sim 10$ nm for the inter-skyrmion distance $\sim 50$ nm reported in Ref. [50], and the temperature $T = 70$ K. The induced transverse heat flux changes its direction as the net spin density varies across zero, at which magnons of two chiralities are degenerate and thus the thermal Hall effect is absent similarly to antiferromagnets [27]. When the spin density is negative, for example, there are more positive-chirality magnons than the others, causing the negative thermal Hall conductivity as shown in Fig. 3(b).

Next, let us estimate the change of the thermal Hall conductivity $\Delta\kappa^{yx}$ as the net spin density $s$ varies by $\Delta s \sim 5\times 10^{-8}$ J·s/m$^3$, which can be achieved by changing the temperature by $\Delta T = 10$ K around CP of GdFeCo films according to the numerical results in Ref. [25]. Here, we assume that all the parameters except the spin density are constant. By using the inertia $\rho \sim \hbar^2/Jd^3$ obtained with the Heisenberg exchange energy $J \sim 5$ meV and the lattice constant $d \sim 0.5$ nm, the above $\Delta s$ yields $\Delta\kappa^{yx} \sim 0.05$ W/K·m for 50-nm thick films, which is comparable to the large thermal Hall conductivities observed in frustrated magnets [51].

*Discussion.*—Let us discuss approximations used in this work. First, in obtaining the magnon bands [Eq. (11)] shown in Fig. 2 from the equation of motion [Eq. (3)], we have used the approximation of the uniform fictitious magnetic field by assuming sufficiently closely packed skyrmions [37]. Second, for the numerical estimation of the variation of the thermal Hall conductivity, we assumed that all the other materials parameters $\rho$, $A$, and $D$ than the spin density $s$ are constant. We would like to remark here that our main experimental prediction that the thermal Hall conductivity $\kappa^{yx}$ changes its sign across CP where $s$ flips its sign can be deduced from time-reversal symmetry property of the magnon equation of motion [Eq. (3)] and thus does not rely on these two approximations. In addition, our theory of magnonic Landau levels is applicable to materials with sufficiently small damping and weak disorder so that mean free path of magnons is much longer than the inter-skyrmion distance, and thus than the magnetic length.

S.K.K. acknowledges the enlightening discussions with Oleg Tchernyshyov and Ari Turner. We also thank anonymous referees for the valuable comments that helped us improve the manuscript. S.K.K. and Y.T. were supported by the Army Research Office under Contract No. W911NF-14-1-0016. K.N. was supported by Leading Initiative for Excellent Young Researchers, MEXT, Japan. D.L. was supported by the Swiss National Science Foundation, the NCCR QSIT, and JSPS KAKENHI Grant Numbers 16K05411.

[1] A. N. Bogdanov and D. A. Yablonskii, Sov. Phys. JETP **68**, 101 (1989); A. Bogdanov and A. Hubert, J. Magn. Magn. Mater. **138**, 255 (1994).

[2] N. Nagaosa and Y. Tokura, Nat. Nanotechnol. **8**, 899 (2013), and references therein.

[3] M. Lee, W. Kang, Y. Onose, Y. Tokura, and N. P. Ong, Phys. Rev. Lett. **102**, 186601 (2009); A. Neubauer, C. Pfleiderer, B. Binz, A. Rosch, R. Ritz, P. G. Niklowitz, and P. Böni, Phys. Rev. Lett. **102**, 186602 (2009).

[4] O. Gomonay, V. Baltz, A. Brataas, and Y. Tserkovnyak, Nat. Phys. **14**, 213 (2018), and references therein.

[5] S. Woo, K. M. Song, X. Zhang, Y. Zhou, M. Ezawa, X. Liu, S. Finizio, J. Raabe, N. J. Lee, S.-I. Kim, S.-Y. Park, Y. Kim, J.-Y. Kim, D. Lee, O. Lee, J. W. Choi, B.-C. Min, H. C. Koo, and J. Chang, Nat. Commun. **9**, 959 (2018); S. Woo, K. M. Song, X. Zhang, M. Ezawa, Y. Zhou, X. Liu, M. Weigand, S. Finizio, J. Raabe, M.-C. Park, K.-Y. Lee, J. W. Choi, B.-C. Min, H. C. Koo, and J. Chang, Nat. Electron. **1**, 288 (2018).

[6] L. Caretta, M. Mann, F. Büttner, K. Ueda, B. Pfau, C. M. Günther, P. Hessing, A. Churikova, C. Klose, M. Schneider, D. Engel, C. Marcus, D. Bono, K. Bagschik, S. Eisebitt, and G. S. D. Beach, Nat. Nanotechnol. (2018).

[7] Y. Hirata, D.-H. Kim, S. K. Kim, D.-K. Lee, S.-H. Oh, D.-Y. Kim, T. Nishimura, T. Okuno, Y. Futakawa, H. Yoshikawa, A. Tsukamoto, Y. Tserkovnyak, Y. Shiota, T. Moriyama, S.-B. Choe, K.-J. Lee, and T. Ono, (2018), arXiv:1809.00415.

[8] T. Jungwirth, X. Marti, P. Wadley, and J. Wunderlich, Nat. Nanotechnol. **11**, 231 (2016), and references therein.

[9] V. Baltz, A. Manchon, M. Tsoi, T. Moriyama, T. Ono, and Y. Tserkovnyak, Rev. Mod. Phys. **90**, 015005 (2018), and references therein.

[10] L. Šmejkal, Y. Mokrousov, B. Yan, and A. H. MacDonald, Nat. Phys. **14**, 242 (2018).

[11] P. M. Buhl, F. Freimuth, S. Blügel, and Y. Mokrousov, Phys. Status Solidi RRL **11**, 1700007 (2017), 1700007; C. A. Akosa, O. A. Tretiakov, G. Tatara, and A. Manchon, (2017), arXiv:1709.02931.

[12] B. Göbel, A. Mook, J. Henk, and I. Mertig, Phys. Rev. B **95**, 094413 (2017).

[13] B. Göbel, A. Mook, J. Henk, and I. Mertig, New J. Phys. **19**, 063042 (2017).

[14] B. Göbel, A. Mook, J. Henk, and I. Mertig, Phys. Rev. B **96**, 060406(R) (2017).

[15] F. Bloch, Z. Physik **61**, 206 (1930); T. Holstein and H. Primakoff, Phys. Rev. **58**, 1098 (1940).

[16] A. V. Chumak, V. I. Vasyuchka, A. A. Serga, and B. Hillebrands, Nat. Phys. **11**, 453 (2015), and references therein.

[17] D. D. Sheka, I. A. Yastremsky, B. A. Ivanov, G. M. Wysin, and F. G. Mertens, Phys. Rev. B **69**, 054429 (2004); V. K. Dugaev, P. Bruno, B. Canals, and C. Lacroix, Phys. Rev. B **72**, 024456 (2005).

[18] M. Garst, J. Waizner, and D. Grundler, J. Phys. D: Appl. Phys. **50**, 293002 (2017), and references therein.

[19] K. A. van Hoogdalem, Y. Tserkovnyak, and D. Loss, Phys. Rev. B **87**, 024402 (2013).

[20] K. Nakata, J. Klinovaja, and D. Loss, Phys. Rev. B **95**, 125429 (2017).

[21] C. Schütte and M. Garst, Phys. Rev. B **90**, 094423 (2014); Y.-T. Oh, H. Lee, J.-H. Park, and J. H. Han, Phys. Rev. B **91**, 104435 (2015); Y. Onose, T. Ideue, H. Katsura, Y. Shiomi, N. Nagaosa, and Y. Tokura, Science **329**, 297 (2010); Y. Shiomi, R. Takashima, and E. Saitoh, Phys. Rev. B **96**, 134425 (2017).

[22] A. Kirilyuk, A. V. Kimel, and T. Rasing, Rep. Prog. Phys. **76**, 026501 (2013), and references therein.

[23] C. D. Stanciu, A. V. Kimel, F. Hansteen, A. Tsukamoto, A. Itoh, A. Kirilyuk, and T. Rasing, Phys. Rev. B **73**, 220402 (2006).

[24] M. Binder, A. Weber, O. Mosendz, G. Woltersdorf, M. Izquierdo, I. Neudecker, J. R. Dahn, T. D. Hatchard, J.-U. Thiele, C. H. Back, and M. R. Scheinfein, Phys. Rev. B **74**, 134404 (2006).

[25] K.-J. Kim, S. K. Kim, Y. Hirata, S.-H. Oh, T. Tono, D.-H. Kim, T. Okuno, W. S. Ham, S. Kim, G. Go, Y. Tserkovnyak, A. Tsukamoto, T. Moriyama, K.-J. Lee, and T. Ono, Nat. Mater. **16**, 1187 (2017).

[26] S. K. Kim, K.-J. Lee, and Y. Tserkovnyak, Phys. Rev. B **95**, 140404(R) (2017); S.-H. Oh, S. K. Kim, D.-K. Lee, G. Go, K.-J. Kim, T. Ono, Y. Tserkovnyak, and K.-J. Lee, Phys. Rev. B **96**, 100407(R) (2017).

[27] K. Nakata, S. K. Kim, J. Klinovaja, and D. Loss, Phys. Rev. B **96**, 224414 (2017).

[28] G. E. W. Bauer, E. Saitoh, and B. J. van Wees, Nat. Mater. **11**, 391 (2012).

[29] S. K. Kim and Y. Tserkovnyak, Appl. Phys. Lett. **111**, 032401 (2017).

[30] Although we considered only one type of spin-orbit coupling, $\propto \mathbf{n}\cdot(\boldsymbol{\nabla}\times\mathbf{n})$, in this work, our main results of the magnonic Landau levels and the ensuing thermal Hall effect are valid as long as the ferrimagnet is in the skyrmion crystal phase regardless of the type of spin-orbit coupling.

[31] J. H. Han, J. Zang, Z. Yang, J.-H. Park, and N. Nagaosa, Phys. Rev. B **82**, 094429 (2010); O. Petrova and O. Tchernyshyov, Phys. Rev. B **84**, 214433 (2011); S. Banerjee, J. Rowland, O. Erten, and M. Randeria, Phys. Rev. X **4**, 031045 (2014).

[32] B. Ivanov and A. Sukstanskii, Solid State Commun. **50**, 523 (1984); D. Loss, D. P. DiVincenzo, and G. Grinstein, Phys. Rev. Lett. **69**, 3232 (1992).

[33] Microscopically, the parameter $\rho$ is given by $\rho = s_{\rm sat}^2\chi_\perp$ where $s_{\rm sat}$ is the saturated spin density (e.g., $s_{\rm sat} = (|s_1| + |s_2|)/2$ for two-sublattice ferrimagnets with sublattice spin densities $s_1$ and $s_2$) and $\chi_\perp$ is the transverse magnetic susceiptiblity [9, 25, 26].

[34] A. F. Andreev and V. I. Marchenko, Sov. Phys. Usp. **23**, 21 (1980).

[35] A. A. Kovalev and Y. Tserkovnyak, Europhys. Lett. **97**, 67002 (2012); A. A. Kovalev, Phys. Rev. B **89**, 241101(R) (2014).

[36] The generators for three-dimensional rotations can be defined in terms of the Levi-Civita symbol as follows: $(\mathcal{L}_a)_{bc} = -\epsilon_{abc}$, where $a, b$, and $c$ are indices for spatial coordinates, $x, y$, and $z$.

[37] Supplemental Material contains the derivation of the equations of motion for magnons, the summary of the known results for the Landau levels of a charged particle, and the discussion on the approximation of the uniform fictitious magnetic field, which includes Ref. [52].

[38] G. E. Volovik, J. Phys. C: Solid State Phys. **20**, L83 (1987); C. H. Wong and Y. Tserkovnyak, Phys. Rev. B **80**, 184411 (2009); J. Zang, M. Mostovoy, J. H. Han,

and N. Nagaosa, Phys. Rev. Lett. **107**, 136804 (2011).
[39] E. G. Tveten, A. Qaiumzadeh, and A. Brataas, Phys. Rev. Lett. **112**, 147204 (2014).
[40] R. Cheng and Q. Niu, Phys. Rev. B **86**, 245118 (2012).
[41] Here, we remark that all the potential terms, $\phi, \mathbf{a}^t$, and $\mathbf{a}^d$, are functions of the material parameters such as $A$, $D$, and $\mathbf{h}$.
[42] E. Schrödinger, Ann. Physik **81**, 109 (1926); W. Gordon, Z. Physik **40**, 117 (1926); O. Klein, *ibid.* **41**, 407 (1927); S. K. Kim, Y. Tserkovnyak, and O. Tchernyshyov, Phys. Rev. B **90**, 104406 (2014); A. Qaiumzadeh, L. A. Kristiansen, and A. Brataas, Phys. Rev. B **97**, 020402 (2018).
[43] R. Cheng, M. W. Daniels, J.-G. Zhu, and D. Xiao, Sci. Rep. **6**, 24223 (2016).
[44] A. A. Belavin and A. M. Polyakov, JETP Lett. **22**, 245 (1975).
[45] S. M. Girvin, "The quantum hall effect: Novel excitations and broken symmetries," in *Topological aspects of low dimensional systems*, edited by A. Comtet, T. Jolicœur, S. Ouvry, and F. David (Springer, Berlin, Heidelberg, 1999), and references therein.
[46] L. Lam, J. Math. Phys. **12**, 299 (1971).
[47] S. Murakami and A. Okamoto, J. Phys. Soc. Jpn. **86**, 011010 (2017), and references therein.
[48] D. Xiao, M.-C. Chang, and Q. Niu, Rev. Mod. Phys. **82**, 1959 (2010), and references therein.
[49] In this Letter, we do not include the effects of the nonequilibrium magnon accumulation on the thermal magnon transport, which can be important in a system with appropriate boundary conditions as shown in Ref. [20].
[50] X. Z. Yu, Y. Onose, N. Kanazawa, J. H. Park, J. H. Han, Y. Matsui, N. Nagaosa, and Y. Tokura, Nature **465**, 901 (2010); S. Seki, X. Z. Yu, S. Ishiwata, and Y. Tokura, Science **336**, 198 (2012).
[51] M. Hirschberger, J. W. Krizan, R. J. Cava, and N. P. Ong, Science **348**, 106 (2015); M. Hirschberger, R. Chisnell, Y. S. Lee, and N. P. Ong, Phys. Rev. Lett. **115**, 106603 (2015).
[52] D. P. Xue and G. Xiao, Phys. Rev. B **45**, 5986 (1992).